LU TAN-1 SAR SATELLITE CHARACTERISTICS AND PRODUCTIONS IN THE PHASE OF IN-ORBIT TEST

Tao Li[1], Xinming Tang[1,], Xiaoming Gao[1], Xiang Zhang[1], Xuefei Zhang[1], Jing Lu[1], Tao Chen[1,2], Xiaohong Qiao[1,3], Jing Han[1,4], Zheng Li[1,5]*

[1] Land Satellite Remote Sensing Application Center, Ministry of Natural Resources, Beijing 100048, China;
[2] Surveying and Mapping Data Archives of Guizhou Province;
[3] Yunan Remote Sensing Center;
[4] Shaanxi Satellite Application Center for Natural Resources;
[5] Geological Technical Information Center of Yunnan Province.

KEY WORDS: Lu Tan-1, In-Orbit Test, Platform, Payload, Digital Elevation Model, Deformation.

ABSTRACT:

Lu Tan-1 (LT-1) has finished the in-orbit test and will be delivered to the users in 2023. In this paper, we discussed the satellite characteristics including the satellite mission, the platform as well as the payload. The satellite constellation was designed following two main demands, i.e., digital elevation model (DEM) generation and deformation monitoring. Thus, we provided two kinds of productions. First was the DEM created using the images provided by helix bistatic formation. Second was the deformation products created using that of pursuit monostatic formation. The deformation products were finally classified into three different types given the processing technologies. They were deformation field provided by differential interferometric SAR (InSAR, DInSAR), deformation velocity field provided by stacking, and deformation time series provided by multi-temporal InSAR. DEM data were validated to be better than 5 m compared to ICESat. Deformation field, deformation velocity field, as well as deformation time series were validated to be better than 2.7 mm, 8.6 mm/yr and 3.7 mm, respectively.

1. BACKGROUND

Lu Tan-1 (LT-1), also named as L-band differential interferometric synthetic aperture radar (SAR, InSAR, DInSAR), were launched on 20220126 (YYYYMMDD) and 20220227 separately(Li et al. 2022a). LT-1 is a constellation consists of LT-1 A and LT-1 B. LT-1 B was launched to the orbit with orbital phase angle difference of 45 degrees from LT-1 A. Then the satellites were tested for about three months separately. At the end of June, the terrain mapping test task starts using the helix bistatic formation (HBF). At the end of 2022, LT-1 converted to the pursuit monostatic formation (PMF) to start the

Figure 1. Formations of LT-1. (a) shows helix bistatic formation used for DEM generation, and (b) shows pursuit monostatic formation used for deformation monitoring.

* Corresponding author.

deformation test task, see Fig. 1. Three months were expected to be used for deformation monitoring. There are two main tasks for LT-1, i.e., digital elevation model (DEM) generation and deformation monitoring. The first task is used to provide terrain information in the cloud-prone and rainy regions that are not possible to be captured by the optical satellites. The second is the primary task used to provide deformation information in the highly and moderately susceptive geohazard areas (HIMSGA) of China(Li et al. 2022b).

2. SATELLITE CHARACTERISTICS

2.1 Satellite Platform

The satellite platform was designed to follow the strictly regressive orbit (SRO)(Du et al. 2018). Which was used to ensure the orbital tube radius as small as 350 m. Orbit was designed by applying the layer-by-layer iterative formation. The J2 regression was used to determine the orbit parameters on the basis of 90 orders gravity field iterative corrections and meet the precise revisit accuracy requirements. Both LT-1 A and LT-1 B satellites were equipped with identical GNSS receiver. It mainly consists of power supply, frequency reference unit, low noise processing, global navigation satellite system (GNSS) information processing, and interface connection functional modules. The GNSS receivers supported GPS, BD2 and BD3 system signals from the antenna. Besides GPS L1&L2 and BDS B1I&B3I signals, we also supported the tracking of new signals B1C and B2A of BD system. The GNSS signals were transmitted to the digital signal processing part. The digital signal processor obtained the original observation data by acquisition, tracking and demodulation process. It will also complete navigation, positioning, and absolute timing.

2.2 Satellite Payload

The payload of LT-1 featured the active phased array antenna of high performance and the multi-mode signal generator. The antenna was splitted into two halves in along-track direction that allows for receiving different polarizations at the same time or imaging with high resolution and wide swath(Lin et al. 2022). The signal generator could generate the general linear frequency modulated chirp signal. Main parameters of the payload are listed in Tab. 1.

Parameter	Value		
Frequency	L-band		
Bandwidth	Up to 84 MHz		
Antenna	9.8 m × 3.4 m		
Polarization	Single/dual/quad/compact		
Peak Power	16000 W		
Workmode	Mode	Resolution	Swath width
	Stripmap 1	3 m	50 km
	Stripmpa 2	12 m	100 km
	Stripmap 3	6 m	30 km
	Stripmap 4	24 m	160 km
	ScanSAR	30 m	400 km
Incidence Angle	10°- 60° 20°- 46° for interferometry		

Table 1. Primary Payload Parameters.

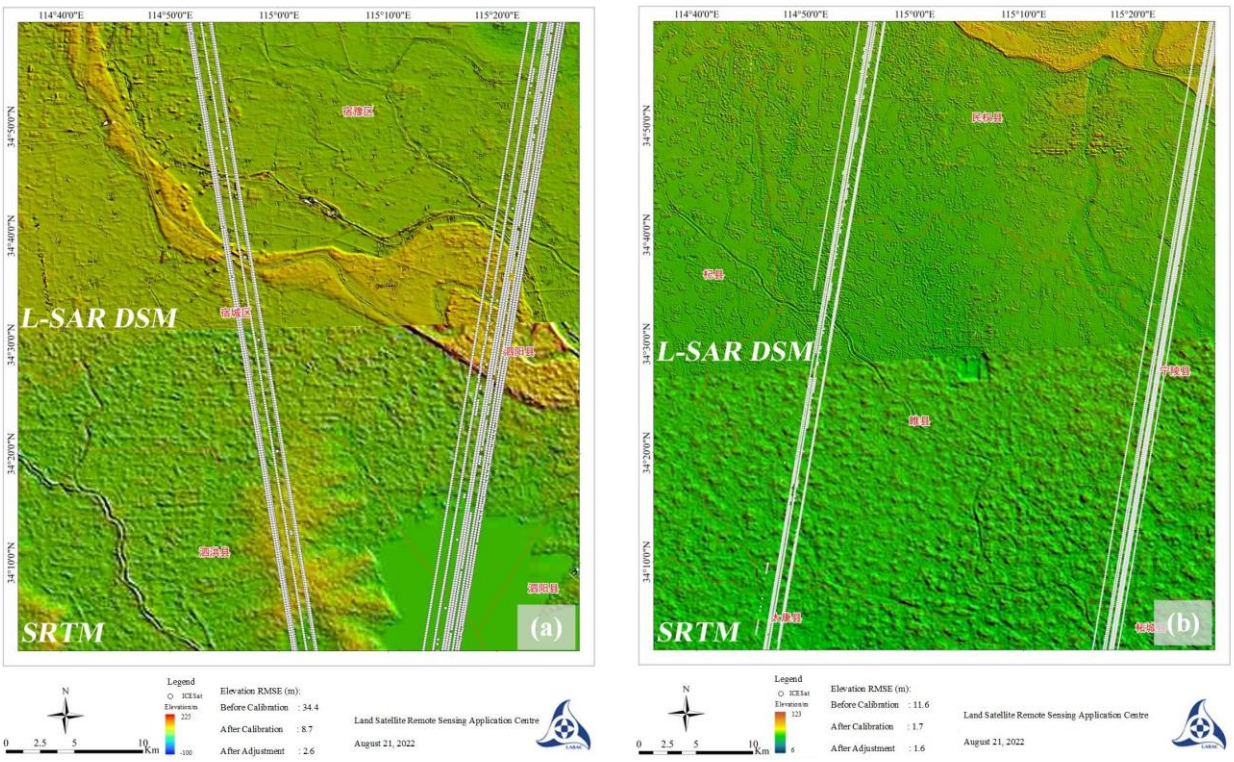

Figure 2. DEM generated over (a) Shangqiu of Henan Province and (b) Suqian of Jiangsu Province. White points are ICESat data.

3. DEM AND DEFORMATION PRODUCTS ASSESSMENT

3.1 DEM Production

DEM products obtained by LT-1 are shown in Fig. 2. We have also shown the shuttle radar topography mission (SRTM) DEM below LT-1 DEM in Fig. 2. The DEM products were mosaiced without plain inconsistency, meaning that the geometric parameters are equal to each other. The in-orbit test result of the geometric accuracy was better than 4 meters. While the plain accuracy of SRTM DEM was better than 13 meters(Farr et al. 2007). Pixel spacing after geocoding was 12 meters for us and 30 meters for SRTM. Therefore, the geometric error induced pixel distortion less than 1 pixel. And the resolution of LT-1 DEM was apparently better than SRTM. The root mean square error (RMSE) of Henan DSM before calibration was 11.6 m, that after calibration was 1.7 m. We used the Ice, Cloud, and Land Elevation Satellite (ICESat) altimeter payload to remove the height ramp w.r.t. the phase ramp induced by interferometric parameters error residues including range, azimuth timing, baseline, phase, PAC positioning, and so on. Final height accuracy after removing the systematic error was 1.6 m. And that of Suqian, Jiangsu were 34.4 m, 8.7 m and 2.6 m, respectively.

Shangqiu and Suqian were selected as the calibration fields. We obtained the interferometric baseline bias using the two fields, and then the parameters were used to calculate the other interferograms. Fig. 3 show different DEM products covering flat ground in Nantong of Jiangsu, hills in Handan of Hebei, mountainous and alpine regions in Chengdu of Sichuan, respectively. Histograms of DEM error compared to TanDEM-DEM were also provided in the figure. No obvious bias observed in the histograms. Accuracy of the three regions were 1.24 m, 0.94 m and 4.71 m if calculated without ground control points. If we used ICESat data as ground control points to conduct adjustment, thus removing the systematic error affected by the baseline residue, phase residue, slat range residue and so on, we could further improve the accuracy to 1.00 m, 0.68 m and 2.53 m. Accuracy at 1:50,000 measurement scale was required by us, which is around 5 m in hilly regions. After assessment, we believe that those three regions pre-selected before satellite launch fulfils the needs.

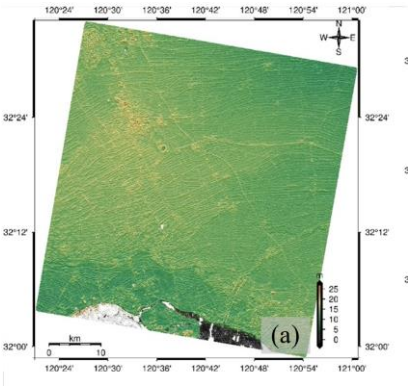

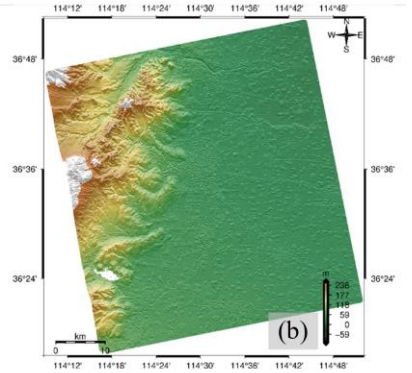

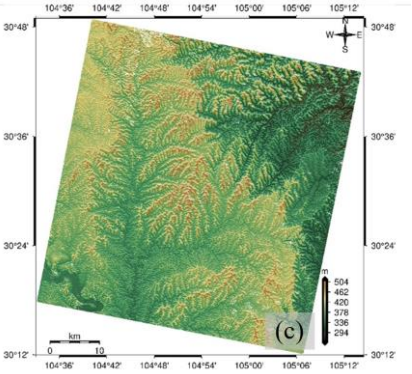

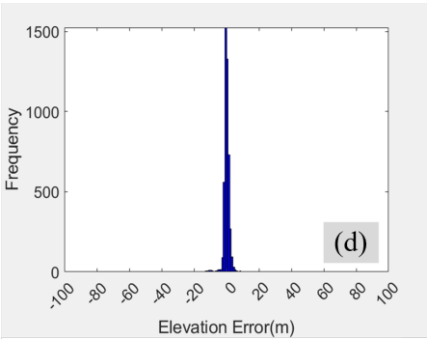

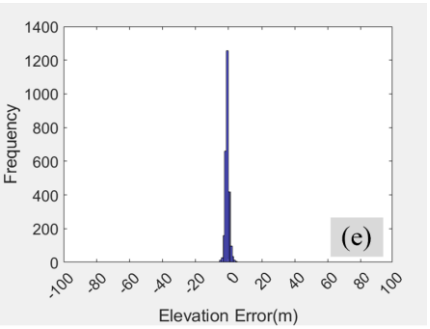

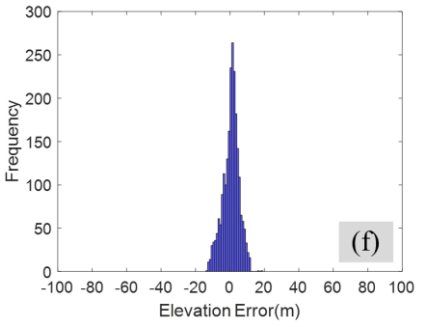

Figure 3. DEM calculate using the interferograms covering (a) Nantong of Jiangsu Province, (b) Handan of Hebei Province, (c) Chengdu of Sichuan Province. (d) (e) and (f) are the corresponding histograms of DEM error compared to TanDEM-X DEM, respectively.

3.2 Deformation Products

Three deformation products were pre-defined for the satellite. They were deformation field product calculated using DInSAR, deformation velocity field product calculated using stacking, and deformation time series product calculated using multi-temporal InSAR (MTInSAR) (Li et al. 2022b; Tao Li 2023).

Fig. 4 was the first deformation phenomena of LT-1 caused by the ice surface movement. The imaging dates were 20220226 and 20220306. Temporal baseline was only 8 days. The relative movement in LOS deformation exceeded 0.8 m. We concluded that the ice surface moved toward different directions. Given that the image was descending data, the blue regions were those moving from west to east, the red regions were those moving from east to west. Now we are planning to obtain more data covering the Tuosuo Lake.

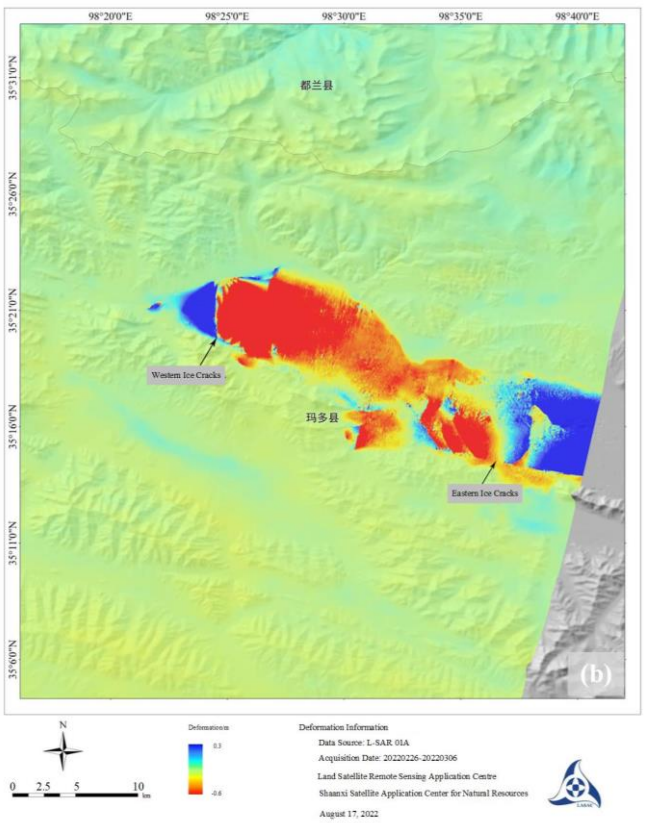

Figure 4. The first LOS deformation captured by LT-1 over Tuosuo Lake in Qinghai Province.

Fig. 5 (a) shows the deformation fields in Datong City of Shanxi Province, there were totally 71 subsiding funnels in the region. The maximum LOS deformation was 0.5 m between the imaging dates of 20221215 and 20230116, meaning that the maximum LOS deformation velocity was about 1.1 cm/day. People living here were relocated to avoid the potential threaten. We used the levelling data which were taken while the satellite flying over the test area. The levelling points were plotted using black triangles. RMSE of the product was 2.7 mm.

Fig. 5(b) is the deformation velocity field obtained between 20230116 and 20230418, 13 images have been collected over the time lag. Results were compared to the levelling data, RMSE of 8.6 mm/yr are obtained.

Fig. 5(c) is the deformation time series calculated using small baseline subset (SBAS) method over a coal mine in the research area. We tried to arrange the levelling points along and across the coal mine excavation direction. In Fig. 5 (f), we obtained the comparison result between SBAS and levelling along the coal mine excavation direction. While Fig 5(g) is that across the coal mine excavation direction. Accuracy was calculated using the overall data. RMSE was 3.7 mm.

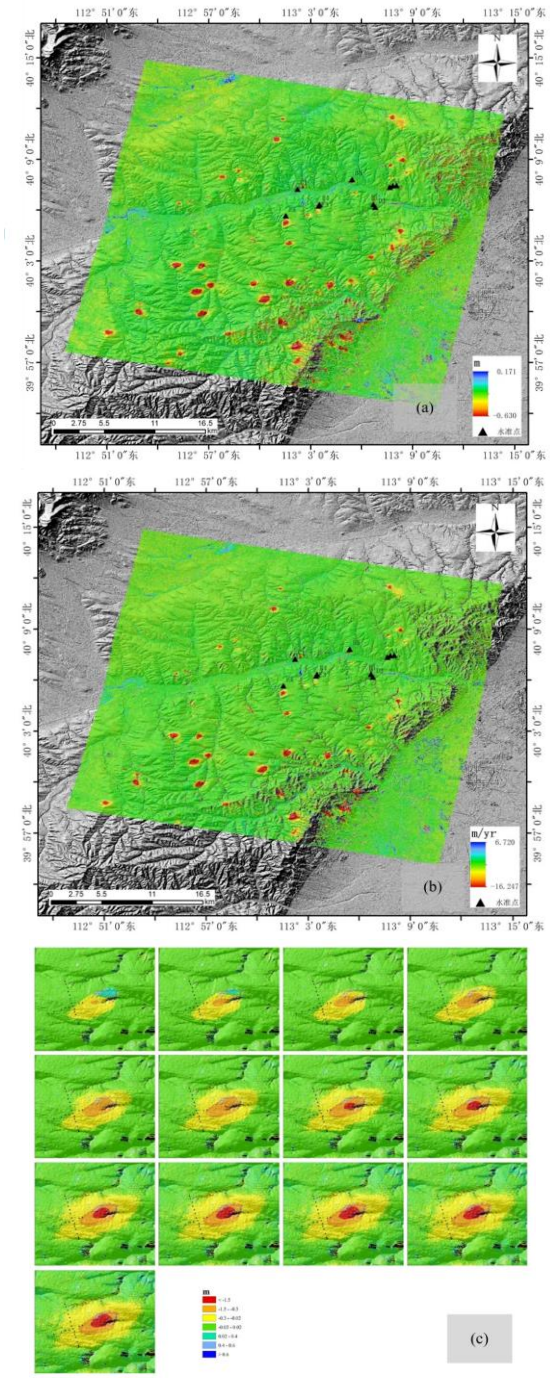

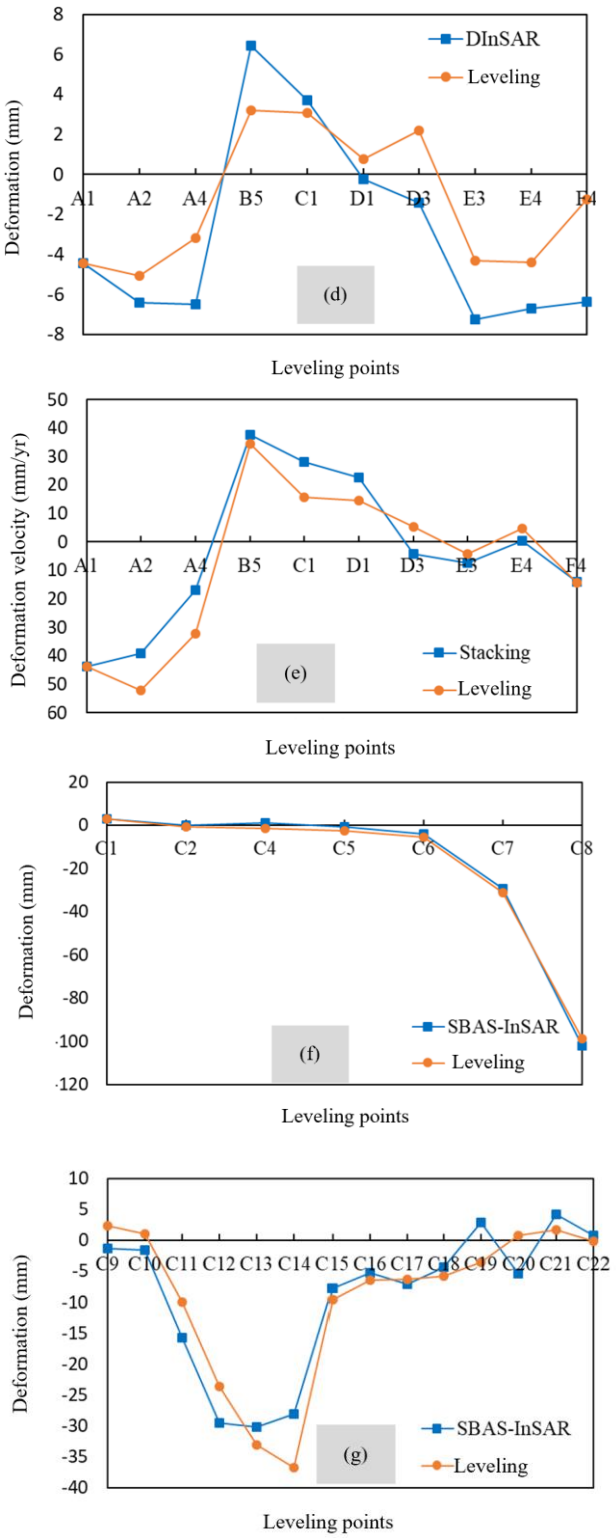

Figure 5. Deformation products and assessments. (a) is the deformation field calculated using DInSAR. (b) is the deformation velocity field calculate using stacking. (c) is the deformation time series calculated using MTInSAR. (d) is the deformation comparison between deformation field and levelling data, (c) is that of deformation velocity field, (d) and (e) are two characteristic lines of a coal mine of deformation time series. Black triangles are the levelling data.

4. CONCLUSIONS

LT-1 is the first Chinese satellite constellation used for deformation monitoring. In this paper, we showed some satellite characteristics of the satellite platform and payload. Especially, we provided the first DEM products and deformation products. The DEM products were better than 1:50,000 measurement scale. While the deformation field calculated using DInSAR was better than 2.7 mm. The deformation velocity field calculated using stacking was better than 8.6 mm/yr. And the deformation time series calculated using MTInSAR was better than 3.7 mm.

However, some of the problems are still remains to be solved. First, DEM products over large areas are to be generated using LT-1. In-orbit test only tells the accuracy in the test regions that are pre-selected before satellite launch. We believe that the selected regions are typical and is capable of assessing the satellite quality. However, the DEM quality sometimes relies on the Earth cover. We need to further assess the DEM data in other regions.

Second, deformation products are to be assessed both in different regions and using different methods. Like DEM data which are affected by the undulation and coverage of the Earth surface, deformation products suffer more. DInSAR is quick but affected both by the baseline decoherence, volume decoherence as well as the temporal decoherence. The three decoherence phenomena are supressed by L-band which is used in LT-1. However, atmospheric delay is difficult to be removed even we use GACOS in products generation. Stacking is a better technology which decreases the atmospheric affects. MTInSAR is expected to be best. However, there are two many methods including PSInSAR(Ferretti et al. 2001), PSI(Hooper et al. 2007), SBAS(Berardino et al. 2002), ISBAS(Bateson et al. 2015), TCPInSAR(Zhang 2012), et al. Meanwhile, the distributed scatterer methods have already been developed (Ferretti et al. 2011). It is difficult but necessary to assessed the accuracy and applicability thoroughly given all those methods, thus generating a standard that can be followed by the government users.

The primary working mode of LT-1 in the following years are to be determined. We are now mainly considering the efficiency and the accuracy of stripmap 1 and stripmap 2. The primary mode will soon be selected and kept permanently till the end of the satellite life. Data can be searched in our Natural Resources Satellite Remote Sensing Cloud Service Platform (LASAC and BSIT 2023). With more and more data obtained by LT-1, stacking and multi-temporal InSAR technology will be more and more precise to perform the constantly deformation monitoring in HIMSGA of China.

ACKNOWLEDGEMENTS

Our work has been supported by National Key R&D Programme of China (2021YFC3000405), National Natural Science Foundation (41901303), The Civil Spaceflight Pre-Research Projects (D010206).

REFERENCES

Bateson, L., Cigna, F., Boon, D., & Sowter, A. (2015). The application of the Intermittent SBAS (ISBAS) InSAR method to the South Wales Coalfield, UK. *International Journal of Applied Earth Observation and Geoinformation, 34*, 249-257

Berardino, P., Fornaro, G., Lanari, R., & Sansosti, E. (2002). A new algorithm for surface deformation monitoring based on small baseline differential SAR interferograms. *IEEE Transactions on Geoscience and Remote Sensing, 40*, 2375−2383

Du, Y., Yang, S., Wan, B., Wang, W., & Chen, J. (2018). Strictly-regressive orbit maintenance control of near earth satellites. *Acta Aeronautica et Astronautica Sinica, 38*, 322449

Farr, T.G., Rosen, P.A., Caro, E., Crippen, R., Duren, R., Hensley, S., Kobrick, M., Paller, M., Rodriguez, E., Roth, L., Seal, D., Shaffer, S., Shimada, J., Umland, J., Werner, M., Oskin, M., Burbank, D., & Alsdorf, D. (2007). The shuttle radar topography mission. *Reviews of Geophysics, 45*, 361-393

Ferretti, A., Fumagalli, A., Novali, F., Prati, C., Rocca, F., & Rucci, A. (2011). A new algorithm for processing interferometric data-stacks: SqueeSAR. *IEEE Transactions on Geoscience and Remote Sensing, 49*, 3460−3470

Ferretti, A., Prati, C., & Rocca, F. (2001). Permanent scatterers in SAR interferometry. *IEEE Transactions on Geoscience and Remote Sensing, 39*, 8−20

Hooper, A., Segall, P., & Zebker, H. (2007). Persistent scatterer interferometric synthetic aperture radar for crustal deformation analysis, with application to Volcán Alcedo, Galápagos. *Journal of Geophysical Research, 112*

LASAC, & BSIT (2023). Natural Resources Satellite Remote Sensing Cloud Service Platform. In http://sasclouds.com/chinese/home/

Li, T., Tang, X., Zhou, X., & Zhang, X. (2022a). LuTan-1 SAR Main Applications and Products. In, *EUSAR 2022*. Leipzig, Germany

Li, T., Tang, X., Zhou, X., Zhang, X., Li, S., & Gao, X. (2022b). Deformation Products of Lutan-1(LT-1) SAR Satellite Constellation for Geohazard Monitoring. In, *IGARSS 2022*. Kuala Lumpur, Malaysia: IEEE

Lin, H., Deng, Y., Zhang, H., Liu, D., Liang, D., Fang, T., & Wang, R. (2022). On the Processing of Dual-Channel Receiving Signals of the LuTan-1 SAR System. *Remote Sensing, 14*, 515

Tao Li, X.T., Shijin Li, Xiaoqing Zhou, Xiang Zhang, Yaozong Xu (2023). Classification of basic deformation products of L-band differential interferometric SAR satellite. *Acta Geodaetica et Cartographica Sinica, 52*, 769-779

Zhang, L. (2012). Temporarily Coherent Point SAR Interferometry. In (p. 117): The Hong Kong Polytechnic University